High-Density MIM Capacitors Using $AlTaO_x$ Dielectrics

M. Y. Yang, C. H. Huang, Albert Chin, *Senior Member, IEEE*, Chunxiang Zhu, *Member, IEEE*, M. F. Li, *Senior Member, IEEE*, and Dim-Lee Kwong

***Abstract*—The authors have obtained good MIM capacitor integrity of high-capacitance density of 10 fF/μm^2 using high-κ $AlTaO_x$ fabricated at 400 °C. In addition, small voltage dependence of capacitance of $<$ 600 ppm (quadratic voltage coefficient of only 130 ppm/V^2) is obtained at 1 GHz using their mathematical derivation from measured high-frequency S parameters. These good results ensure the high-κ $AlTaO_x$ MIM capacitor technology is useful for high-precision circuits operated at the RF frequency regime.**

***Index Terms*—Capacitor, dielectric constant, frequency dependence, high κ, MIM, RF.**

I. Introduction

ACCORDING to the ITRS roadmap, the continuously increasing MIM capacitor density $\varepsilon_0\kappa/t_d$[1], [2] is required to achieve a smaller chip area and lower IC cost. Thus, searching for proper high-κ dielectrics [3]–[11] is the primary challenge because decreasing dielectric thickness (t_d) will increase the unwanted leakage current exponentially. The other challenge is how to achieve the small voltage dependence of capacitance $\Delta C/C$ or quadratic voltage coefficient that is the key factor for a precision analog capacitor [7], [8]. In addition, to measure the $\Delta C/C$ at RF frequency is highly desired because the operation speed of the circuit using a precision MIM capacitor is increased to gigahertz as continuous technology evolution. Previously, we have shown a relatively high capacitance density of 5 fF/μm^2 using high-κ Al_2O_3 with good MIM capacitor integrity [9]. In this paper, we have further increased the capacitance density to 10 fF/μm^2 using high-κ $AlTaO_x$. In addition, we also found that the $\Delta C/C$ decreases by orders of magnitude to $<$ 600 ppm as increasing frequency into the gigahertz regime, using our mathematically derived $\Delta C/C$ from high-frequency S parameters. The small $\Delta C/C$ at RF frequency ensures this MIM capacitor technology is useful for high-precision circuits at this frequency regime.

Manuscript received January 27, 2003; revised February 28, 2003. This work was supported by NSTB/EMT/TP/00/001.2. The review of this letter was arranged by Editor C.-P. Chang.

M. Y. Yang, C. H. Huang, and A. Chin are with the Department of Electronics Engineering, National Chiao Tung University, Hsinchu, Taiwan, R.O.C.

C. Zhu and M. F. Li are with the Silicon Nano Device Lab, Department of Electrical and Computer Engineering, National University of Singapore, 119260 Singapore.

D.-L. Kwong is with the Department of Electrical and Computer Engineering, The University of Texas, Austin, TX 78752 USA (e-mail: achin@cc.nctu.edu.tw).

Digital Object Identifier 10.1109/LED.2003.812572

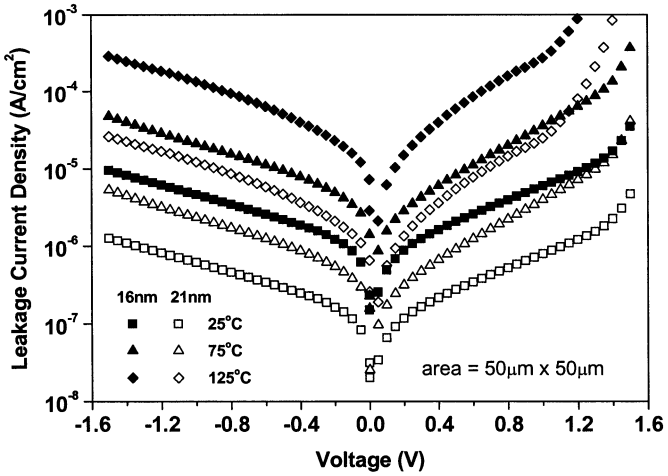

Fig. 1. J–V characteristics of 16 and 21 nm $AlTaO_x$ MIM capacitors. Voltage is applied to bottom Pt electrode.

II. Experiment

After growing 500-nm isolation SiO_2 on 4-in Si wafers, the bottom Pt–Ti metal electrode and transmission line are formed. Then, a thin Al:Ta (1:6) layer was deposited by physical vapor evaporation on the bottom Pt–Ti, followed by subsequent oxidation for 45 min and annealing for 15 min at 400 °C to form high-κ $AlTaO_x$. Two $AlTaO_x$ thicknesses of 16 and 21 nm are measured by an ellipsometer. The motivation for adding Al into $AlTaO_x$ is to achieve good capacitor integrity with Al_2O_3 dielectric [7], [9], [10]. Finally, Al metal was used for both top capacitor electrode and transmission line with 50 μm$\times$ 50 μm capacitor area. The $AlTaO_x$ MIM capacitors were characterized by HP4284A LCR meter from 10 KHz to 1 MHz and measured by S parameters using an HP8510C network analyzer from 200 MHz to 30 GHz followed by standard deembedding from a dummy device [10]–[15]. Additionally, the transmission line with the same length without a capacitor is used for deembedding the parasitic transmission line related substrate loss [13], [14].

III. Results and Discussion

Fig. 1 shows the J–V characteristics of $AlTaO_x$ MIM capacitors. The leakage current decreases with increasing the $AlTaO_x$ thickness and reducing temperature. The asymmetrical J–V under positive and negative bias is due to the different work function of top Al and bottom Pt electrodes. Leakage currents of 4.4×10^{-7} and 3.6×10^{-6} A/cm^2 are measured at room temperature and -1 V applied to Pt electrode that is

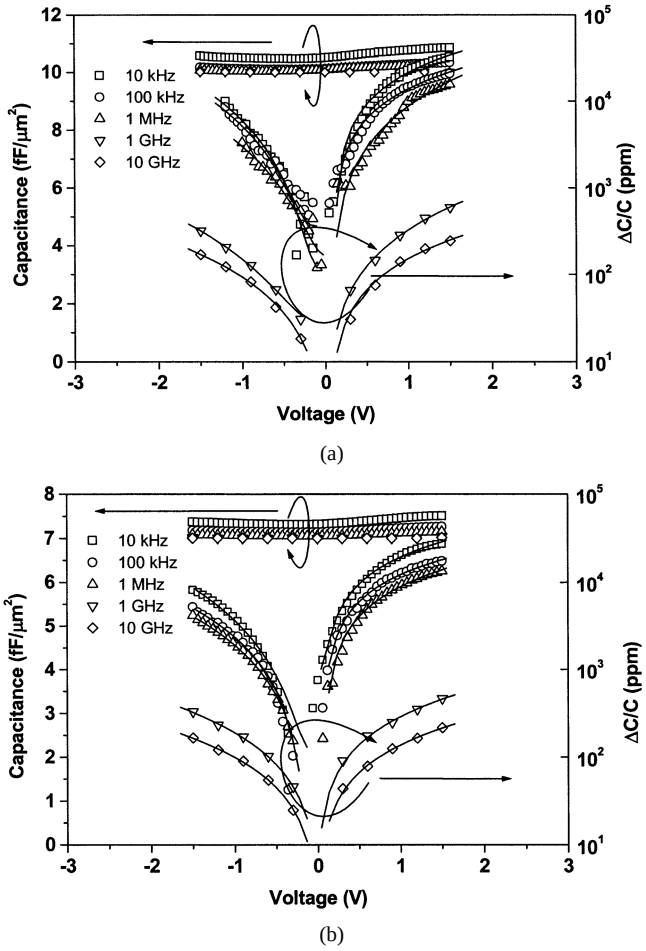

Fig. 2. C–V characteristics of (a) 16- and (b) 21-nm $AlTaO_x$ MIM capacitors at different frequencies from 10 kHz to 10 GHz. The voltage is applied to the bottom Pt electrode. Measured area is 50 μm × 50 μm.

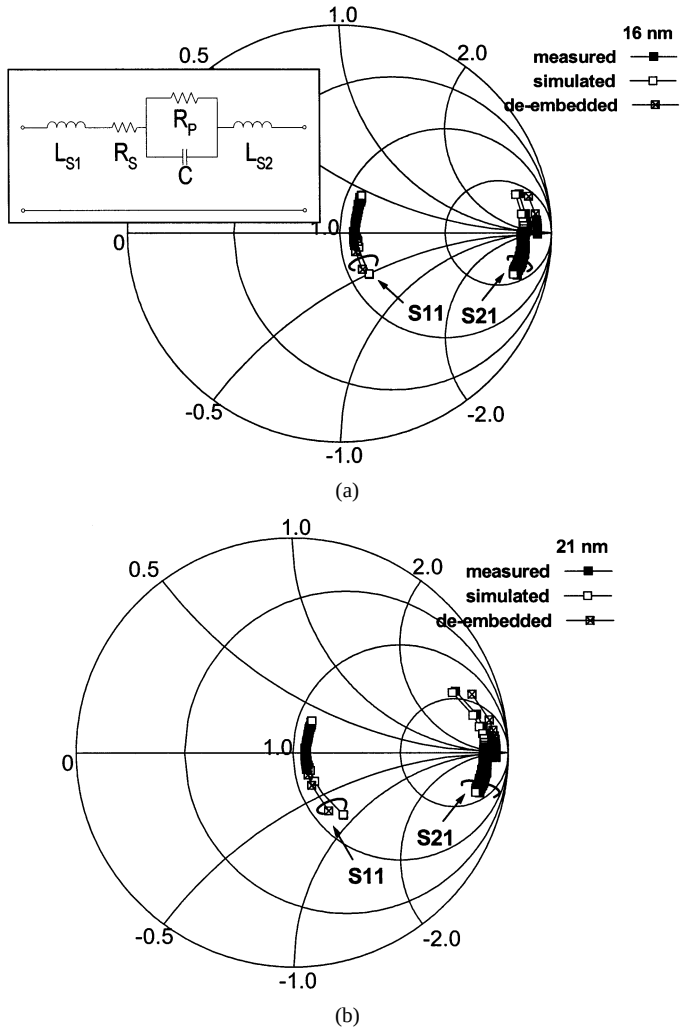

Fig. 3. Measured and simulated S parameters of (a) 16- and (b) 21-nm $AlTaO_x$ MIM capacitors. Figure is the equivalent circuit model. Deembedded S parameters from transmission line are also shown.

much better than the previous $AlTiO_x$ case [9]. A possible reason may be due to the larger energy bandgap for Ta_2O_5 than TiO_2[16]–[18].

Fig. 2(a) and (b) depicts the C–V characteristics and $\Delta C/C$ for $AlTaO_x$ MIM capacitors, with physical thickness of 16 and 21 nm, respectively. High-capacitance densities of 10.3 and 7.2 μF/cm^2 are measured for respective thickness devices at 100 KHz and a κ value of 18 is obtained. It is noticed that the $\Delta C/C$ is worse for thinner $AlTaO_x$ thickness t_d, although it gives a higher C from $\varepsilon_0\kappa/t_d$. Using the Al electrode also gives poorer $\Delta C/C$ than Pt, which has the same trend as the higher leakage current shown in Fig. 1. The measured temperature coefficient of capacitance (TCC) is also higher at thinner thickness, with TCC values of 564, 333, and 255 ppm/°C for 16 nm device and 356, 237, and 156 ppm/°C for the 21-nm device for 10 KHz, 100 KHz, and 1 MHz, respectively. It is noticed that both TCC and $\Delta C/C$ decrease monotonically with $\ln(1/C)$, and comparable values are obtained with previous HfO_2 data [8] at the same $1/C$ by extrapolation. Such exponential dependences of TCC and $\Delta C/C$ decrease with $1/C$ and should have important physical meanings; they are currently under investigation.

To further study the $\Delta C/C$ and high-frequency characteristics beyond the measurement capability of the precision LCR meter, we have measured the S parameters up to 30 GHz. Fig. 3 shows the measured and modeled S parameters for $AlTaO_x$ MIM capacitors. The insert figure is the equivalent circuit model, where R_S, L_S, R_P, and C are the parasitic series resistor, parasitic series inductor, parallel resistor, and capacitor, respectively. Good matching between measured and modeled S parameters is obtained for $AlTaO_x$ MIM capacitors with two different thicknesses. This indicates the good accuracy of the physically based model. The $\Delta C/C$ at RF frequency is shown in (1), which can be obtained by differentiating the measured S_{21}[19] shown in (2)

$$\frac{\Delta C}{C} = \frac{Z_0\left(2+\frac{Z}{Z_0}\right)^2}{2R_P^2} j\omega C\left(R_p + \frac{1}{j\omega C}\right)^2 \Delta(S_{21}) \quad (1)$$

$$S_{21} = \frac{2}{2+\frac{Z}{Z_0}} \quad (2)$$

$$Z = R_s + j\omega(L_{s1}+L_{s2}) + \frac{\frac{R_p}{j\omega C}}{R_p + \frac{1}{j\omega C}}. \quad (3)$$

Z and Z_0 in (2) and (3) are the total impedance and characteristic impedance of the transmission line. The derived $\Delta C/C$ at

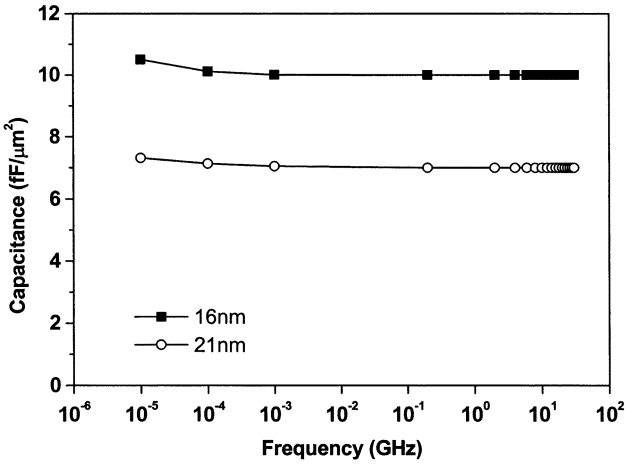

Fig. 4. Frequency-dependent capacitance of 16- and 21-nm $AlTaO_x$ MIM capacitors.

1 and 10 GHz are also shown in Fig. 2. The $\Delta C/C$ decreases monotonically by orders of magnitude with increasing frequency from 10 KHz to 10 GHz. This small $\Delta C/C < 600$ ppm (or quadratic voltage coefficient of only 130 ppm/V^2) at 1 GHz suggests the high-κ $AlTaO_x$ can be useful for a high-precision MIM capacitor and circuits [20] at this frequency regime.

Fig. 4 shows the frequency-dependent capacitance reduction for the high-κ $AlTaO_x$ MIM capacitor. A small capacitance reduction of 5% is obtained from 10 KHz to 30 GHz. The larger capacitance value at a low frequency of 10 KHz, in combination with the fast $\Delta C/C$ reduction at higher frequency, suggests the mechanism may be defect-related because the slow traps may not have enough speed to follow the high-frequency signals [13], [14], [21]. However, the small capacitance reduction high-capacitance density and small $\Delta C/C < 600$ ppm fit all the requirements for a MIM capacitor at RF frequencies.

IV. Conclusion

We have achieved high 10 fF/μm^2 capacitance density and small $\Delta C/C < 600$ ppm at 1 GHz using high-κ $AlTaO_x$ processed at 400 °C. The good device integrity should find application for precision circuit at high frequencies.

References

[1] J. A. Babcock, S. G. Balster, A. Pinto, C. Dirnecker, P. Steinmann, R. Jumpertz, and B. El-Kareh, "Analog characteristics of metal-insulator-metal capacitors using PECVD nitride dielectrics," *IEEE Electron Device Lett.*, vol. 22, pp. 230–232, May 2001.

[2] C.-M. Hung, Y.-C. Ho, I.-C. Wu, and K. O, "High-Q capacitors implemented in a CMOS process for low-power wireless applications," in *IEEE MTT-S Int. Microwave Symp.*, 1998, pp. 505–511.

[3] S. J. Lee, H. F. Luan, C. H. Lee, T. S. Jeon, W. P. Bai, Y. Senzaki, D. Roberts, and D. L. Kwong, "Performance and reliability of ultra thin CVD HfO_2 gate dielectrics with dual poly-Si gate electrodes," in *Proc. Symp. VLSI Technology*, 2001, pp. 133–134.

[4] L. Kang, Y. Jeon, K. Onishi, B. H. Lee, W.-J. Qi, R. Nieh, S. Gopalan, and J. C. Lee, "Single-layer thin HfO_2 gate dielectric with n+-polysilicon gate," in *Proc. Symp. VLSI Technology*, 2000, pp. 44–45.

[5] A. Chin, C. C. Liao, C. H. Lu, W. J. Chen, and C. Tsai, "Device and reliability of high-κ Al_2O_3 gate dielectric with good mobility and low D_{it}," in *Proc. Symp. VLSI Technology*, 1999, pp. 133–134.

[6] M. Y. Yang, S. B. Chen, A. Chin, C. L. Sun, B. C. Lan, and S. Y. Chen, "One-transistor PZT/Al_2O_3, SBT/Al_2O_3 and BLT/Al_2O_3 stacked gate memory," in *IEDM Tech. Dig.*, 2001, pp. 795–798.

[7] H. Hu, C. Zhu, X. Yu, A. Chin, M. F. Li, B. J. Cho, and D. L. Kwong, "MIM capacitors using atomic-layer-deposited high-κ $(HfO_2)_{1-x}(Al_2O_3)_x$ dielectrics," *IEEE Electron Device Lett.*, vol. 24, pp. 60–62, Feb. 2003, to be published.

[8] H. Hu, C. Zhu, Y. F. Lu, M. F. Li, B. J. Cho, and W. K. Choi, "A higher performance MIM capacitors using HfO_2 dielectrics," *IEEE Electron Device Lett.*, vol. 23, pp. 514–516, Sept. 2002.

[9] S. B. Chen, J. H. Chou, A. Chin, J. C. Hsieh, and J. Liu, "High density MIM capacitors using Al_2O_3 and $AlTiO_x$ dielectrics," *IEEE Electron Device Lett.*, vol. 23, pp. 185–187, Apr. 2002.

[10] S. B. Chen, J. H. Chou, K. T. Chan, A. Chin, J. C. Hsieh, and J. Liu, "Frequency-dependent capacitance reduction in high-κ $AlTaO_x$ and Al_2O_3 gate dielectrics from IF to RF frequency range," *IEEE Electron Device Lett.*, vol. 23, pp. 203–205, Apr. 2002.

[11] S. B. Chen, J. H. Chou, A. Chin, J. C. Hsieh, and J. Liu, "RF MIM capacitors using high-κ Al_2O_3 and $AlTiO_x$ dielectrics," in *IEEE MTT-S Int. Microwave Symp.*, vol. 1, 2002, pp. 201–204.

[12] K. T. Chan, A. Chin, Y. B. Chen, Y.-D. Lin, D. T. S. Duh, and W. J. Lin, "Integrated antennas on Si, proton-implanted Si and Si-on-quartz," in *IEDM Tech. Dig.*, 2001, pp. 903–906.

[13] K. T. Chan, A. Chin, C. M. Kwei, D. T. Shien, and W. J. Lin, "Transmission line noise from standard and proton-implanted Si," in *IEEE MTT-S Int. Microwave Symp.*, 2001, pp. 763–766.

[14] Y. H. Wu, A. Chin, K. H. Shih, C. C. Wu, C. P. Liao, S. C. Pai, and C. C. Chi, "RF loss and crosstalk on extremely high resistivity (10 K-1 MΩ-cm) Si fabricated by ion implantation," in *IEEE MTT-S Int. Microwave Symp.*, 2000, pp. 221–224.

[15] Y. H. Wu, A. Chin, C. S. Liang, and C. C. Wu, "The performance limiting factors as RF MOSFET's scale down," in *Radio Frequency Integrated Circuits Symp.*, 2000, pp. 151–155.

[16] H. H. Kung, H. S. Jarrett, A. W. Sleight, and A. Ferretti, "Semiconducting oxide anodes in photoassisted electrolysis of water," *J. Appl. Phys.*, vol. 48, no. 6, pp. 2463–2469, 1977.

[17] E. Franke, C. L. Trimble, M. J. DeVries, and J. A. Woollam, "Dielectric function of amorphous tantalum oxide from the far infrared to the deep ultraviolet spectral region measured by spectroscopic ellipsometry," *J. Appl. Phys.*, vol. 88, no. 9, pp. 5166–5174, 2000.

[18] K. H. Yoon and K. B. Park, "Dependence of photoelectric behavior of TiO_2 electrodes on processing variables," *J. Appl. Phys.*, vol. 64, no. 4, pp. 2189–2193, 1988.

[19] D. M. Pozar, *Microwave Engineering*. New York: Wiley, 1998, pp. 208–209.

[20] "Process integration, devices, & structure," in *International Technology Roadmap for Semiconductors*, 2001 ed., pp. 18–19.

[21] K. K. Hung, P. K. Ko, C. Hu, and Y. C. Cheng, "A unified model for the flicker noise in metal-oxide-semiconductor field-effect transistor," *IEEE Trans. Electron Devices*, vol. 37, pp. 654–665, Mar. 1990.